Original Research

Magnetic Resonance Elastography of Skeletal Muscle

M. Alex Dresner, MS,[1] Gregory H. Rose, MD, PhD,[2] Phillip J. Rossman, MS,[1] Raja Muthupillai, PhD,[3] Armando Manduca, PhD,[1] and Richard L. Ehman, MD[1]*

While the contractile properties of skeletal muscle have been studied extensively, relatively little is known about the elastic properties of muscle in vivo. Magnetic resonance elastography (MRE) is a phase contrast-based method for observing shear waves propagating in a material to determine its stiffness. In this work, MRE is applied to skeletal muscle under load to quantify the change in stiffness with loading. A mathematical model of muscle is developed that predicts a linear relationship between shear stiffness and muscle load. The MRE technique was applied to bovine muscle specimens (N = 10) and human biceps brachii in vivo (N = 5). Muscle stiffness increased linearly for both passive tension (14.5 ± 1.77 kPa/kg) and active tension, in which the increase in stiffness was dependent upon muscle size, as predicted by the model. A means of noninvasively assessing the viscoelastic pro-perties of skeletal muscle in vivo may provide a useful method for studying muscle biomechanics in health and disease. J. Magn. Reson. Imaging 2001;13:269–276. © 2001 Wiley-Liss, Inc.

Index terms: muscle; elastography; contraction; mechanical properties; magnetic resonance imaging

ALTHOUGH SKELETAL MUSCLE IS CRUCIAL for normal human function, little is known about the elastic properties of this tissue in vivo. If such properties could be characterized noninvasively, it could provide a means of diagnosing or monitoring several diseases that affect skeletal muscle, such as degenerative myopathies, stroke, and diabetes. It has been observed that a number of muscle properties are affected by disease, e.g., muscle fiber density, motor unit potential, motor nerve conduction velocity, muscle strength (peak isometric and isokinetic contraction), and muscle endurance (1–4). Unfortunately, most of these assessment methods are invasive. For example, an electroneuromyogram requires an electrical impulse to be introduced into the muscle via inserted electrodes. It would be desirable to have a noninvasive means to evaluate muscle function to decide a course of treatment for a disease such as multiple sclerosis, to determine the best rehabilitation program for stroke patients, and to evaluate strength training regimes (3). Mechanical testing devices can be developed to determine viscoelastic properties in vivo, but these evaluate entire musculoarticular systems rather than isolated muscles (5) and must be developed individually for each joint to be tested. Ultrasound-based approaches have been used to assess the response of the tissue to applied stress to estimate tissue mechanical properties (6,7). Levinson et al. (8) applied vibration sonoelastography to study skeletal muscle and observed that muscle stiffness depends on applied load and stress frequency. Vibration sonoelastography studies are limited in frequency range by the spatial resolution of the ultrasound scan, and limited in motion sensitization to the Doppler detection modes of the ultrasound equipment. The speckle inherent in ultrasound imaging limits the minimum resolvable wavelength in a depth-dependent fashion from approximately 1 cm near the transducer to several centimeters at 10–15 cm depth. Over the range of shear wave frequencies useful for imaging in vivo (50–300 Hz), vibration sonoelastography has a minimum resolvable stiffness of 1–40 kPa. The maximum resolvable stiffness depends on the field of view (FOV), which also varies with depth, from the transducer diameter at the transducer face to 15 cm or more at its deepest penetration.

Magnetic resonance elastography (MRE) is a recently described technique (9,10) that can provide estimates of the mechanical properties of tissues, such as shear modulus or Young's modulus. A phase contrast MRI method is used to measure small cyclic displacements caused by externally applied low-frequency shear waves propagating in tissue. From the displacement measurements, the speed and attenuation of shear waves can be determined, and from the shear wave speed the shear modulus can be calculated. A stiff material (one with a high shear modulus) resists local deformations, so the wavelength of the shear wave is long and the shear wave speed is high. The shear wave speed c (meters/second) is given by:

[1]Magnetic Resonance Laboratory, Department of Diagnostic Radiology, Mayo Clinic, Rochester, Minnesota.

[2]Memorial Hermann Hospital SW, Houston, Texas.

[3]Philips Medical Systems, St. Luke's Episcopal Hospital, Houston, Texas.

Contract grant sponsor: NIH; Contract grant numbers: CA75552; HD37650.

*Address reprint requests to: R.L.E., M.D., Magnetic Resonance Laboratory, Mayo Clinic, 200 1st Street SW, Rochester, MN 55905.

Received March 17, 2000; Accepted July 27, 2000.

$$c = f\lambda \quad (1)$$

where f is the frequency of excitation in Hz and λ the shear wavelength in meters. For a simple isotropic, Hookean material, the shear modulus μ is directly related to the shear wave speed c by (11):

$$\mu = \rho c^2 \quad (2)$$

where ρ is the mass density in kg/m^3 and μ is measured in units of pressure, Pascals. So for a known input frequency, estimation of the wavelength of the shear wave yields an estimate of the shear modulus. The shear *modulus* of a material is an absolute quantity that does not vary with the frequency of vibration; we use the term shear *stiffness* to indicate the shear modulus of an object at a specific frequency. The MRE method has been validated for a phantom model using mechanical testing as a standard for determination of shear modulus (9,10). The potential advantages of MRE for evaluating muscle include the high sensitivity of MR to cyclic motion and flexible options for motion and sensitization direction, in imaging plane orientation and shear wave excitation frequency.

The goals of this work were twofold. The primary goal was to adapt MRE to the study of skeletal muscle and undertake a systematic study of the elastic properties of skeletal muscle under loaded conditions. The secondary goal of this work was to develop a mathematical model to predict the behavior of skeletal muscle under load and verify the ex vivo and in vivo experimental results against theoretical predictions.

Our proposed model for the elastic properties of muscle is based on its structure. Each muscle fiber (cell) contains many myofibrils that can be divided longitudinally into repeating subunits, the 2.1 μm sarcomeres. A sarcomere is the fundamental operational unit of a muscle. The mechanism of muscle contraction may be elucidated by describing its action within the framework of the well validated sliding filament theory (12). The sliding filaments are actin and myosin. The myosin filament is comprised of a long, stiff tail and a globular head that points out toward the nearest actin filament. The head can bind to the actin filament to form a "crossbridge" between the filaments. When the actin filament is pulled by the motion of the myosin head (acting through the crossbridge), the sarcomere shortens, and thus the entire muscle fiber shortens. The tension provided by a muscle fiber depends on the number of current actin-myosin crossbridges (13). These crossbridges also determine the shear stiffness of the fiber by binding the stiff actin and myosin filaments together, just as cross-linking the long molecules of a polymer give it rigidity.

Model of Muscle Elasticity

A mathematical model of muscle can be derived from these fundamental principles of muscle structure and of its function. We start by recognizing that muscle has a given value of elasticity when relaxed, so the shear stiffness μ must depend on the passive structures ($g_{passive}$) as well as the stiffness of the contractile apparatus ($f_{contractile}$):

$$\mu = f_{contractile} + g_{passive} \quad (3)$$

The contractile apparatus is not considered to have any contribution to muscle stiffness when the muscle is relaxed.

We next recognize that the crossbridges that generate force in muscle contraction also change the stiffness of the muscle by linking the stiff actin and myosin proteins. For isometric contractions (in which muscle generates a constant force without shortening) the stiffness of the muscle may be taken as a direct indication of the number of active crossbridges in the muscle (14,15). Thus the muscle stiffness in isometric contraction should be linearly related to force generation (where T is active tension in Newtons and α is a proportionality constant):

$$f_{contractile} = \alpha T \quad (4)$$

The total number of crossbridges determines the maximum force that may be generated by the muscle T_{max}. Tetanus, complete muscle contraction, will be reached when the muscle is generating its maximum force and is at its highest possible shear stiffness μ_T. Smaller amounts of force generated would generate a smaller proportion of activated fibers, so the shear stiffness would be a proportion of μ_T. A given load will induce the same number of crossbridges to form for any muscle, but this number will be a larger fraction of the total for a small muscle. T_{max} is linearly related to the muscle volume V (the area, determined by the number of fibers, multiplied by the length, representing the number of sarcomeres in series). Thus the increase in shear stiffness with active contraction will be modulated by the inverse of the volume because a larger volume of muscle will require less shear stiffness increase. This can be represented by substituting α_0/V for the proportionality constant α:

$$f_{contractile} = \alpha_0 \frac{T}{V} = \mu_T \frac{T}{T_{max}} \quad (5)$$

The passive structures of muscle are responsible for its elasticity in the relaxed state, when tension is zero and no force is generated. A larger muscle will have more passive structures (thicker tendons and more connective tissue), so the shear stiffness due to the passive structures will also be some function of the size of the muscle. The spring constant of the passive structures (which may be assumed elastic for a first approximation) will be determined by the cross-sectional area of the muscle:

$$g_{passive} = \frac{k}{A} + C \quad (6)$$

where k is a function with units of force and the constant C represents the stiffness of the relaxed muscle with no tension. Energy of deformation is stored in the

passive structures, so the contribution of the passive structures to the shear stiffness of muscle will not be a constant but will depend on the tension in the muscle. The passive structures of the muscle are under tension if the muscle is elongated or if it is isometrically contracting, because in an isometric contraction the active fibers shorten against the passive structures of the muscle. Not all of the energy of fiber contraction is stored in the passive structures, so a proportionality factor k′ (no units) is added to reflect the partial storage of energy:

$$g_{\text{passive}} = \frac{k'T}{A} + C \quad (7)$$

where T here represents tension applied to the muscle *or* tension generated in the muscle. Returning to the original description of shear stiffness as a sum of contributions from active and passive components, we may write

$$\mu = f_{\text{contractile}} + g_{\text{passive}} = \left(\mu_T \frac{T}{T\,\max}\right) + \left(\frac{k'T}{A} + C\right) \quad (8)$$

Or equivalently

$$\mu = f_{\text{contractile}} + g_{\text{passive}} = \left(\alpha_0 \frac{T}{V}\right) + \left(\frac{k'T}{A} + C\right) \quad (9)$$

From this mathematical model, it is possible to make the following predictions about the mechanical behavior of skeletal muscle under constant tension: 1) The shear stiffness will increase linearly with tension for isometric contraction, but will be positive even for zero tension. 2) The slope of the shear stiffness-load relationship for active contraction will be related to the inverse of the volume and of the cross-sectional area. 3) Passive tension will also produce a linear shear stiffness increase, but the slope will only be dependent on the cross-sectional area.

METHODS

Ex Vivo Studies

To test the accuracy of the model prediction of the effects of tension on the passive structures of muscle, an ex vivo muscle protocol was developed. Bovine peroneus tertius and extensor digitorum longus muscles were removed with their tendon attachments from a euthanized animal. A total of 10 such specimens were studied. Between 12–36 hours after removal the specimen was allowed to reach room temperature, and one tendon was clamped to a fixed block, with the other tendon connected to a cable and pulley system. This set-up (Fig. 1) allowed the muscle to be placed under various amounts of static tension. Shear waves were induced in the muscle with a toothed rod embedded in one end of the muscle. The other end of the rod was attached to an electromechanical driver designed to oscillate vertically. Motion of the probe was thus perpendicular to the muscle fibers. The MRE scan used a

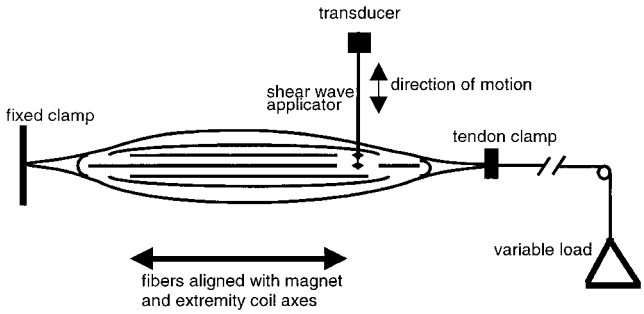

Figure 1. A schematic diagram of the experimental setup for the MRE evaluation of bovine muscle ex vivo. The tendon on one end of the muscle is clamped to a fixed block. The tension applied to the free end of the muscle can be adjusted. The vertical arrow shows the direction of motion of the embedded transducer rod that initiates the shear wave.

gradient-echo implementation of the cyclic motion-sensitive sequence (10), with TR = 100 msec, TE = 26 msec, acquisition matrix = 256 × 64 (with two acquisitions to allow phase image subtraction), and a 20-cm sagittal FOV in a 1.5 Tesla imager (General Electric Medical Systems, Waukesha, WI). The frequency of excitation was 150 Hz, which allowed imaging of several wavelengths within the FOV. Three motion-synchronized gradient pairs were used to increase the sensitivity to the cyclic vertical motion of the propagating shear waves. To allow visualization of the propagating waves, eight images were obtained at phase offsets evenly spaced throughout one 150 Hz cycle by altering the phase relationship between the gradient and the mechanical waveforms, resulting in 1 minute, 44 second scan times. The multiple wave images permitted the propagation of the wave to be visualized and improved the accuracy of the shear stiffness measurements. For each experiment, the applied load was increased from 0 to 14 kg in 2 kg increments. The same section of the muscle was kept within the imaging FOV by physically offsetting the fixed clamp (Fig. 1), to accommodate muscle stretch during the experiment. The driving rod orientation was also carefully maintained throughout the experiment. Ten muscle samples were studied with increasing load applied, to avoid the effects of irreversible muscle damage with high loading.

In Vivo Studies

To assess the predictions for isometrically contracting muscle, volunteer studies (N = 5) were conducted to evaluate the biceps brachii muscle. The biceps brachii muscle was selected because 1) the muscle is fusiform in structure, 2) the volunteer has sufficient fine motor control to decrease motion artifacts, and 3) practical, repeatable loading could be applied with the elbow angle at an optimal 90°. The right arm was used to avoid artifacts arising from chest wall and heart motion. From a supine position, each volunteer was asked to position his right arm as flat as possible by rolling 45° toward the right side (Fig. 2). The transducer plate was placed on the skin above the distal biceps tendon. The volunteer was asked to hold a hand grip attached to the cable

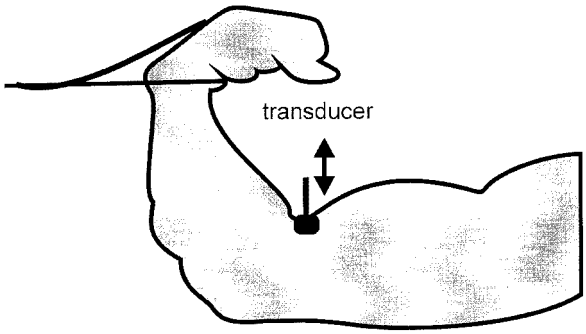

Figure 2. A schematic diagram of the experimental set-up for MRE evaluation of the biceps muscle in vivo. The transducer, attached to the electromechanical driver, is placed on the skin above the biceps tendon. The volunteer holds a loop of cable that runs over a pulley to the desired load. The supine volunteer must remain in this position with the load supported for the duration of the scan time.

(of the pulley system) while keeping his elbow at a 90° angle. The volunteer was expected to maintain the arm position (supporting the load) for each 1 minute, 44 second scan, effectively limiting the number and size of loads tested. A coronal scan plane through the biceps brachii was imaged for 8 phase offsets at each load.

Image Analysis

Each MRE acquisition provides a phase difference image, in which the pixel values are directly proportional to the shear wave displacement at that phase offset and spatial location. Line profiles derived from the phase difference data along the direction of wave propagation were fitted to a damped sinusoid model. The damped sinusoid accounts for the spatial periodicity of the motion as well as the observed attenuation. An example of a line profile and its curve fit is shown in Fig. 3. The estimated wavelength can be converted directly to wave speed c, and thus the shear stiffness may be estimated using Eq. [1], assuming a constant density of 1100 kg/m^3.

RESULTS

Figure 4a, b, and c show a snapshot of the shear wave pattern observed at 150 Hz in a bovine muscle specimen under 2, 8, and 14 kg load, respectively. The change in wavelength with increasing load is apparent. Muscle specimens without tension had low shear stiffness, so at frequencies above 150 Hz wavelengths were too short for good visualization. Specimens under high tension had high shear modulus values, so the wavelength at 150 Hz approached the length of the specimen. The observed shear stiffness of ex vivo bovine muscle as a function of load is shown in Fig. 5. Three different experiments (using different muscle specimens) are included to demonstrate consistency. The shear stiffness was computed for each of the eight phase offsets acquired at each load. Each point on the graph indicates the mean of eight measurements, with the error bars showing ±1 standard deviation of that mean. While variation between specimens was observed, in every case the increase in shear stiffness with load was consistent with a linear relationship. The data in Fig. 5 have a slope of 14.5 ± 1.77 kPa/kg and an R^2 value of 0.92. Each muscle had nearly the same cross-sectional area and length, limiting the effect of cross-sectional area dependence of the passive component in this series of experiments. The shear stiffness without load was measured to be 23.8 ± 6.68 kPa although the intercept of the linear regression was 37.4 kPa. At high loads muscle tearing is expected, and the limit of linear behavior was typically 10 kg for these bovine muscle studies.

In Vivo Studies

Figure 6a shows the wave pattern at a single phase of a shear wave propagating in a coronal section of the biceps (indicated in Fig. 6b) of a healthy volunteer who supported 4 kg of weight for the duration of the scan. The composite image made from the central 10 columns of the wave image from each of the eight phase points enables visualization of the waves propagating through the tissue. Figure 7 shows the shear waves propagating in the biceps muscle of a volunteer supporting weights of 0, 4.0, and 8.0 kg, respectively. Figure 8 shows the relationship between measured shear stiffness and load in volunteers 1, 2, and 4. The slope, intercept, and R^2 values for each of the five volunteers are shown in Table 1. Note the considerable variation in slope and intercept. Volunteer 1 had the largest biceps (27.0 cm^2 cross-sectional area) and volunteer 4 the smallest (11.7 cm^2).

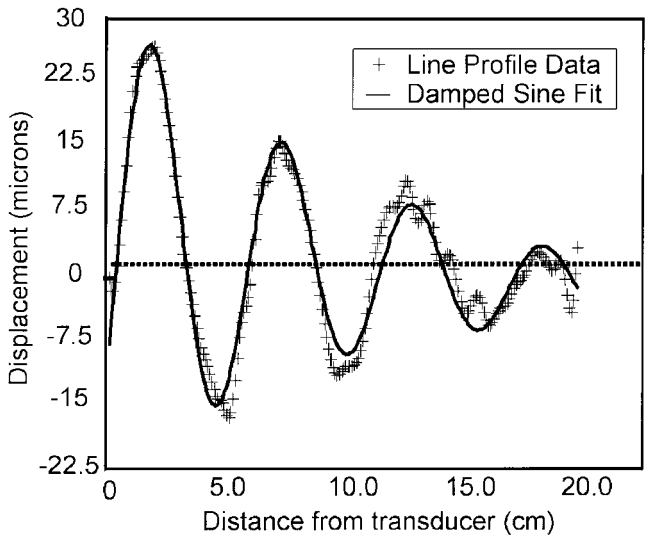

Figure 3. An example of the fit of the line profile data to a damped sinusoid for purposes of wavelength estimation. The line profile was taken from a point near the transducer extending toward the shoulder. The amplitude, attenuation, wavelength, phase, and background level for this profile from a biceps muscle scan were 27.1 μm, 0.113 cm^{-1}, 4.81 cm, –2.02 radians and –0.30 μm, respectively. The wavelength corresponds to a shear stiffness of 52.1 kPa.

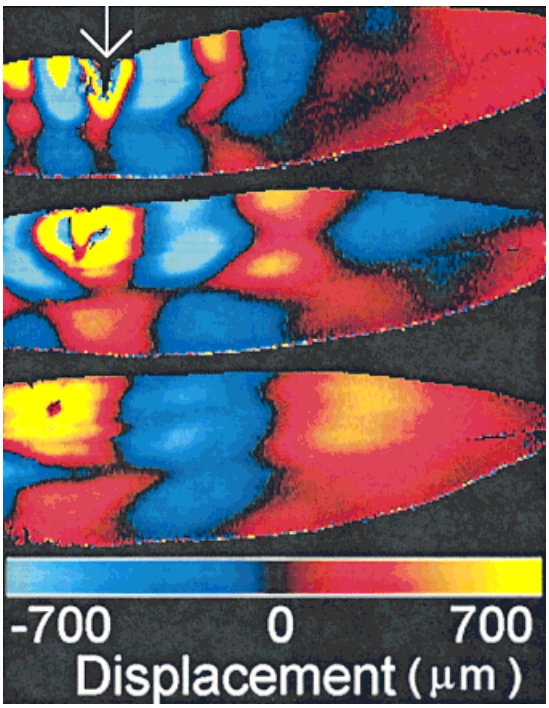

Figure 4. Shear waves observed in a bovine muscle specimen under three different loading conditions. **a:** 2 kg load, demonstrating a short wavelength and high attenuation. **b:** 8 kg load, demonstrating a longer wavelength, less attenuation, and the straightening of the specimen. **c:** 14 kg load, showing a wavelength nearly the length of the specimen and very little attenuation. The wave source location is indicated by the white arrow.

DISCUSSION

The results show that MRE can be used to assess the elastic properties of muscle in specimens and in vivo. The ex vivo results meet the expectation that muscle becomes stiffer as it is stretched, and the in vivo results confirm that muscle contracting against a greater load becomes stiffer. The linearity of the relationships supports the model of muscle presented for both ex vivo passive tension and in vivo isometric contraction. Similar linear increases in the shear stiffness of isolated muscle specimens in vitro with tension have been observed from 50 kPa up to 3 MPa (at 300 Hz) in the biophysical literature (13,15,16) and attributed to both active and passive components of muscle (13,17,18). The passive shear stiffness increase observed in the ex vivo experiments has not been reported previously in the imaging literature.

The shear stiffness of ex vivo muscle measured without load (23.8 ± 6.68 kPa) agrees with both previously published results for whole muscle at room temperature (20,21). The stiffness of ex vivo muscle may be a function of the amount of time between the harvesting of the specimen and the MRE experiment. Even time periods shorter than that necessary for rigor mortis may affect the mechanical properties of ex vivo muscle (22). The discrepancy between the measured and interpolated shear modulus values at zero load may reflect the deviation from linearity in the loading of the muscle at the lower loads, as some tension is required simply to straighten the ex vivo muscle. Previous work has indicated that shear waves traveling in other directions relative to the muscle fiber direction have different shear wave speeds than those that propagate along the fiber direction (20). This requires that the driving rod be kept in a consistent orientation relative to the muscle fibers throughout the experiment for the collected data to be comparable. As the accumulated phase in the MRE experiment is proportional to the dot product of the gradient direction and the motion direction, a change in the motion direction over the course of the experiment (which would occur if the driving rod changed directions) would also alter the amount of accumulated phase, reducing the signal-to-noise ratio of the wave image.

The in vivo stiffness results are in agreement with the published sonoelastography studies (8), which reported similar relationships between shear stiffness and load. Levinson et al. observed an increase in shear stiffness with loading in quadriceps muscles under three different loads at 30, 60, and 120 Hz. Given that frequency, muscle fiber angle, actual muscle strain, and absolute load affect the measured moduli of muscle, direct comparisons of experiments conducted on different muscle groups are difficult, as a 7.5 kg load supported by biceps brachii is very different than one supported by the entire quadriceps muscle group.

The model developed in this study predicted that the proportionality factor for the shear modulus-load relationship be a function of tension, volume, and cross-sectional area. The worst correlation with the linear prediction was that of volunteer 4, who also had the smallest biceps brachii. This volunteer was supporting loads close to his maximum effort level, so the behavior of maximally contracted muscle may deviate from linearity. It is also possible that the two-dimensional imaging of the single coronal imaging plane may not be as accurate for thin muscles. The observed variation in the intercept is not apparently in agreement with the predicted independence of muscle size, though it must be

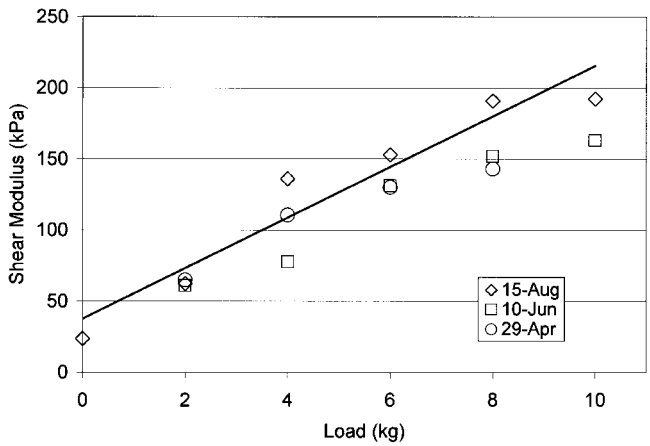

Figure 5. Shear stiffness vs. load for ex vivo muscle. Data from three ex vivo bovine muscle specimens are plotted to demonstrate the linear increase in shear stiffness with tension.

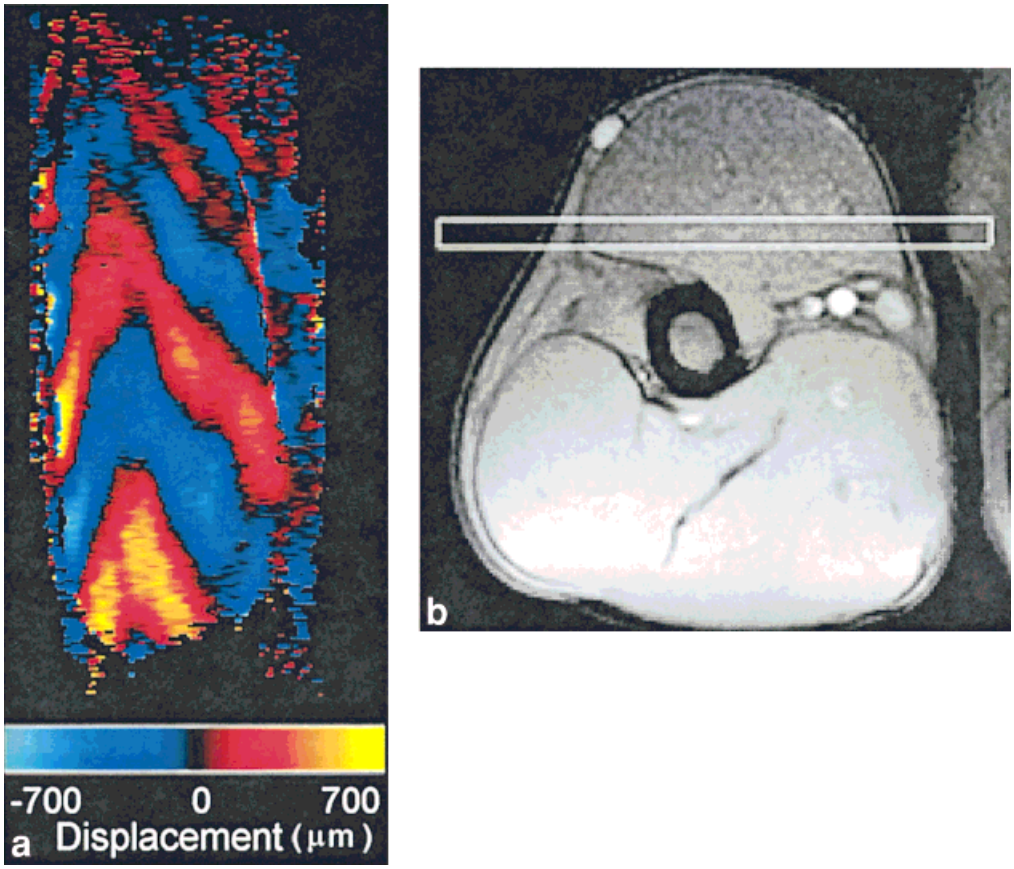

Figure 6. Wave image showing propagating shear waves in the biceps brachii muscle of a volunteer. Image **(a)** was acquired while supporting 4 kg. Image **(b)** is a conventional axial image of the arm, showing the location of the coronal wave image.

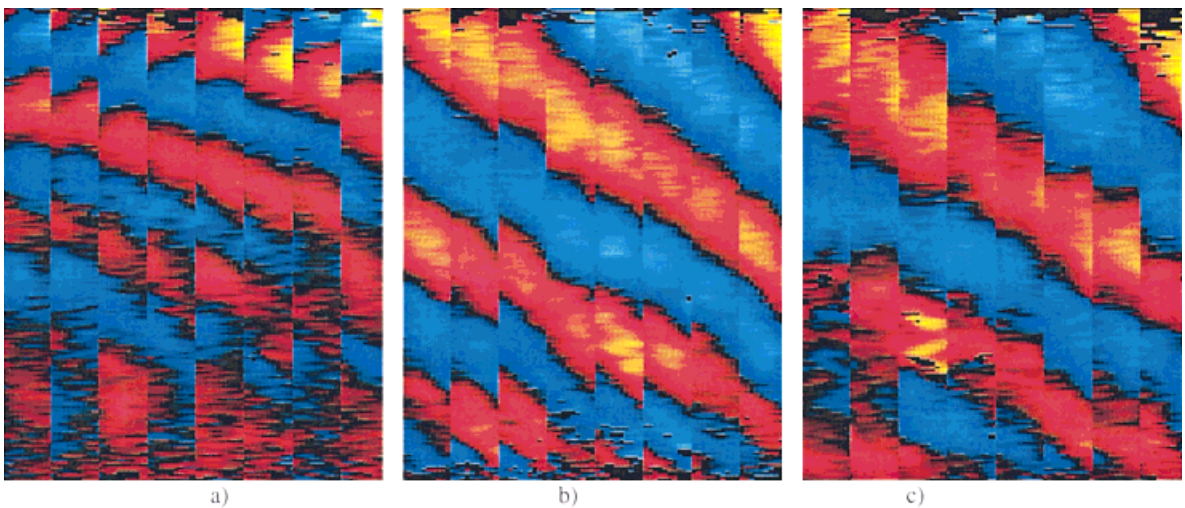

Figure 7. The cine acquisition of the shear waves allows for visualization of the propagating waves in the phase difference images. Each panel consists of columns taken from the same location in the phase difference image at eight phase offsets (of the 150 Hz excitation cycle). Image **(a)** was acquired with no external load, image **(b)** with 4 kg, and image **(c)** with 8 kg. The increase in wavelength with load is readily apparent.

recognized that for the "no load" in vivo case the volunteer held his arm in position, so a minimal amount of active contraction was still present. The observed variation in the slope is consistent with the model presented, as volunteer 1 had the largest biceps and smallest slope (cross-sectional area 27.3 cm^2, slope 7.9 ± 0.4 kPa/kg), volunteer 2 a more average size (cross-sectional area 17.4 cm^2, slope 10.8 ± 1.3 kPa/kg) and volunteer 4 the smallest biceps and a large slope (cross-sectional area 11.7 cm^2, slope 33.1 ± 8.4 kPa/kg). An exact prediction of shear stiffness change with load would require the muscle cross-sectional area, the muscle volume, and location of the biceps tendon attachment, as that is the moment arm which determines the actual tension generated in the biceps for a given load on the hand (23). It is recognized that there are several factors which determine the relationship between weight supported and actual muscle strain, including recruitment of other muscles, muscle volume and cross-sectional area, tendon attachment position, tendon elasticity, and arm length.

The passive tension resistance in muscle (and associated stiffness increase with elongation) arises largely from the elasticity of the protein titin, which binds the myosin filaments in each sarcomere (17,24) (though in an intact muscle the tendons also stretch). This elasticity allows the protein to store the energy of deformation like a spring (24–28). This arrangement requires less total energy for muscle operation as the muscle does work to contract, but stores energy so that relaxation requires no further work. This stored potential energy helps the sarcomeres return to their resting length following a contraction. So increases in muscle stiffness with passive extension should reflect the ability of the connective (rather than contractile) structures to store deformation energy. The passive component of muscle may not be equally adapted to store energy at all strain rates; certainly, bioengineering principles indicate there is no need for efficient energy storage at nonphysiologic frequencies (100 Hz and above). If the ability of the passive component to store energy is dependent upon the frequency of the deformation, then the stiffness will depend on the mechanical excitation frequency used, and dispersion will be observed. Dispersion in actively contracting muscle can be assessed with the same experimental set-up by varying the frequency of mechanical excitation instead of the supported load (20,29).

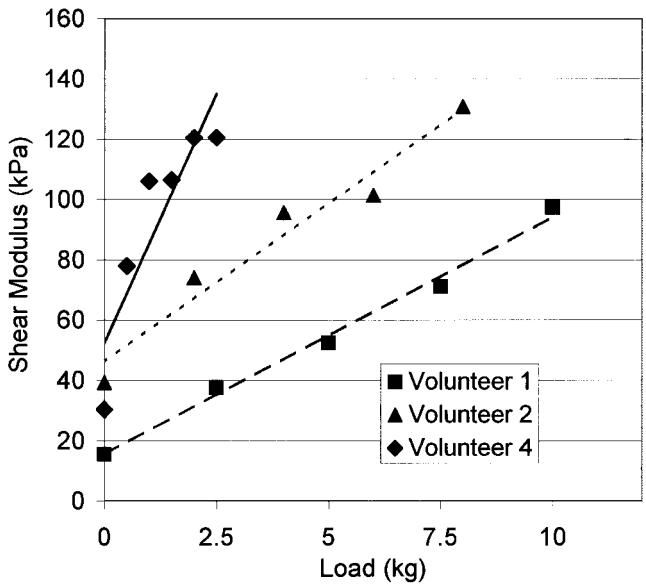

Figure 8. Shear stiffness (in kPa) vs. load (in kg) in vivo. These curves for volunteers 1, 2, and 4 demonstrate the range of slopes measured. Volunteer 1 had the largest biceps brachii in the study (27 cm^2) and volunteer 4 the smallest (11 cm^2).

Table 1
Relationship between Shear Stiffness and Applied Load

Volunteer	Load range (kg)	Slope (kPa/kg)	Intercept, no load (kPa)	R^2
1) 38 y.o. Male	0–10	7.9 ± 0.4	15.6 ± 9.6	0.989
2) 27 y.o. Male	0–8	10.8 ± 1.3	39.2 ± 1.6	0.954
3) 20 y.o. Male	0–5	34.0 ± 3.5	37.7 ± 5.1	0.871
4) 18 y.o. Male	0–2.5	33.1 ± 8.4	30.4 ± 6.1	0.797
5) 55 y.o. Male	0–4	23.2 ± 3.0	14.1 ± 3.8	0.953

With further validation it may be possible to use MRE to assess tension directly. There are a number of biomechanical applications for a tension-mapping tool, including determining which muscle bears load for a given exertion (muscle activation studies) and determining the resting tension distribution in in vivo muscles. While the linear relationship between stiffness and muscle loading has been established previously with isolated muscle fibers (13,15), the distribution of stiffness within a contracting muscle has not been studied for lack of a tool such as MRE. Careful study of passive strain of human muscles could also enable the separate determination of the active and passive components of the increase in shear modulus with tension.

The directional structure of skeletal muscle implies that the shear modulus is not isotropic with respect to the muscle fibers, which has been observed in previous ex vivo and in vivo experiments (20). The static elastic modulus for anisotropic materials is a tensor (μ_{ijkl}) defined by

$$\sigma_{kl} = \mu_{ijkl} u_{ij} \qquad (10)$$

where σ_{kl} and u_{ij} represent the stress and strain tensors. Only one element of that tensor, μ_{yzyz}, has been studied in this work. Because of symmetry considerations in the notation and the physical material (muscle fibers have rotational symmetry about the fiber axis) it can be shown that only six of the 81 coefficients are non-zero and independent (30). We can extend our investigation of wave propagation in muscle to the other components of the shear modulus tensor because MRE imposes no limits on motion generation or sensitization direction. These abilities, combined with the freedom of arbitrary imaging slice orientation relative to the direction of the muscle fibers, will permit a more thorough determination of the wave propagation and mechanical properties. Combination of MRE with techniques that

provide muscle fiber orientation information, such as diffusion tensor imaging (31,32), could optimize MRE parameters with respect to muscle fiber directions and improve the accuracy of the shear modulus determination. This might be necessary for the study of muscles with more complex fiber geometries.

Further applications of MRE might include smooth and cardiac muscle experiments and classification of muscle pathologies. As the shear modulus of muscle rises with passive tension and active contraction, it is possible that this behavior could be used to assess the functionality of a muscle or muscle group. The viability of myocardium is currently assessed by observing cardiac wall motion during the cardiac cycle (33–35), but a shear modulus map indicating areas of high and low tension could also potentially differentiate active from inactive myocardium. Shear modulus estimates may be clinically valuable in assessing the loss of muscle function resulting from degenerative disease. MRE experiments can determine quantitative estimates of the shear stiffness and attenuation characteristics of skeletal muscle, and determine the dependence of these mechanical properties upon muscle load.

ACKNOWLEDGMENTS

The authors thank Thomas Hulshizer for technical assistance.

REFERENCES

1. Andersen H, Stalberg E, Gjerstad MD, Jakobsen J. Association of muscle strength and electrophysiological measures of reinnervation in diabetic neuropathy. Muscle Nerve 1998;21:1647–1654.
2. Grimby G, Stalberg E, Sandberg A, Sunnerhagen KS. An 8-year longitudinal study of muscle strength, muscle fiber size, and dynamic electromyogram in individuals with late polio. Muscle Nerve 1998;21:1428–1437.
3. Sunnerhagen KS, Svantesson U, Lonn L, Krotkiewski M, Grimby G. Upper motor neuron lesions: their effect on muscle performance and appearance in stroke patients with minor motor impairment. Arch Phys Med Rehab 1999;80:155–161.
4. Holder-Powell H, Rutherford, OM. Unilateral lower limb injury: its long-term effects on quadriceps, hamstring and plantarflexor muscle strength. Arch Phys Med Rehab 1999;80:717–720.
5. Tognella F, Mainar A, Vanhoutte C, Goubel F. A mechanical device for studying mechanical properties of human muscles *in vivo*. J Biomech 1997;30:1077–1080.
6. Parker KJ, Huang SR, Musulin RA, Lerner RM. Tissue response to mechanical vibrations for "sonoelasticity imaging". Ultrasound Med Biol 1990;16:241–246.
7. Ophir J, Miller RK, Ponnekanti H, Cespedes I, Whittaker AD. Elastography of beef muscle. Meat Sci 1994;36:239–250.
8. Levinson SF, Shinagawa M, Sato T. Sonoelastic determination of human skeletal muscle elasticity. J Biomech 1995;28:1145–1154.
9. Muthupillai R, Lomas DJ, Rossman PJ, Greenleaf JF, Manduca A, Ehman RL. Magnetic resonance elastography by direct visualization of propagating acoustic strain waves. Science 1995;269:1854–1857.
10. Muthupillai R, Rossman PJ, Lomas DJ, Greenleaf JF, Riederer SJ, Ehman RL. Magnetic resonance imaging of transverse acoustic strain waves. Magn Reson Med 1996;36:266–274.
11. Graff KF. Wave motion in elastic solids. New York: Dover, 1975. p. 276–281.
12. Huxley AF, Simmons RM. Proposed mechanism of force generation in striated muscle. Nature (Lond) 1971;233:533–538.
13. Mason P. Dynamic stiffness and crossbridge action in muscle. Biophys Struct Mech 1977;4:15–25.
14. Ford LE, Huxley AF, Simmons RM. The relation between stiffness and filament overlap in stimulated frog muscle fibres. J Physiol 1981;311:219–249.
15. Morgan D. Separation of active and passive components of short-range stiffness of muscle. Am J Physiol 1977;232:C45–C49.
16. Cole NM, Barry DT. Muscle sound frequencies of the frog are modulated by skeletal muscle tension. Biophys J 1994;66:1104–1114.
17. Blange T, van der Heide UA, Treijtel BW, de Beer EL. The effect of actin filament compliance on the interpretation of the elastic properties of skeletal muscle fibres. J Muscle Res Cell Motil 1997;18:125–131.
18. Bartoo ML, Linke WA, Pollack GH. Basis of passive tension and stiffness in isolated rabbit myofibrils. Am J Physiol 1997;273:C266–276.
19. Moss RL, Halpern W. Elastic and viscous properties of resting frog skeletal muscle. Biophys J 1977;17:213–228.
20. Smith JA, Muthupillai R, Dresner MA, Hulshizer TC, Greenleaf JF, Ehman RL. Tissue characterization using magnetic resonance elastography. Proc Soc Magn Reson Med 1997;3:1903.
21. Bishop J, Poole G, Leitch M, Plewes DB. Magnetic resonance imaging of shear wave propagation in excised tissue. J Magn Reson Imaging 1998;8:1257–1265.
22. Marieb EN. Human anatomy and physiology. Redwood City, CA: Benjamin Cummings, 1995. p. 257.
23. Hobbie RK. Intermediate physics for medicine and biology. New York: John Wiley & Sons, 1988. p. 6–12.
24. Horowits R. The physiological role of titin in striated muscle. Rev Physiol Biochem Pharm 1999;138:57–96.
25. Rief M, Gautel M, Oesterhelt F, Fernandez JM, Gaub HE. Reversible unfolding of individual titin immunoglobulin domains by AFM. Science 1997;276:1109–1112.
26. Linke WA, Ivemeyer M, Mundel P, Stockmeier MR, Kolmerer B. Nature of PEVK-titin elasticity in skeletal muscle. PNAS 1998;95:8052–8057.
27. Improta S, Krueger JK, Gautel M, Atkinson RA, Lefevre JF, Moulton S, Trewhella J, Pastore A. The assembly of immunoglobulin-like modules in titin: implications for muscle elasticity. J Mol Biol 1998;284:761–777.
28. Trombitas K, Greaser M, Labeit S, Jin JP, Kellermayer M, Helmes M, Granzier H. Titin extensibility in situ: entropic elasticity of permanently folded and permanently unfolded molecular segments. J Cell Biol 1998;140:853–859.
29. Fung Y. Biomechanics: mechanical properties of living tissues. New York: Springer-Verlag, 1993. p. 48–55.
30. Landau LD, Lifshitz EM: Theory of elasticity. Boston: Butterworth-Heinemann, 1986. p. 32–37.
31. Reese TG, Weisskoff RM, Smith RN, Rosen BR, Dinsmore RE, Wedeen VJ. Imaging myocardial fiber architecture in vivo with magnetic resonance. Magn Reson Med 1995;34:786–791.
32. Hsu EW, Mori S. Analytical expressions for the NMR apparent diffusion coefficients in an anisotropic system and a simplified method for determining fiber orientation. Magn Reson Med 1995;34:194–200.
33. Zhu Y, Drangova M, Pelc NJ. Fourier tracking of myocardial motion using cine-PC data. Magn Reson Med 1996;35:471–480.
34. Constable RT, Rath KM, Sinusas AJ, Gore JC. Development and evaluation of tracking algorithms for cardiac wall motion analysis using phase velocity MR imaging. Magn Reson Med 1994;32:33–42.
35. Zerhouni EA, Parish DM, Rogers WJ, Yang A, Shapiro EP. Human heart: tagging with MR imaging—a method for noninvasive assessment of myocardial motion. Radiology 1988;169:59–63.